

Comparison of plasma actuator effects under rarefied flow conditions applied to a flat plate and a cylinder

*V. Lago**, *A. Kudryavtsev*** and *J.D. Parisse****

**Laboratoire ICARE, CNRS*

Orléans, France

***2Lab. Computational Aerodynamics, ITAM*

Novosibirsk, Russia

****Polytech'Marseille IUSTI UMR 7343 CNRS-AMU*

Marseille, France

Abstract

This investigation is the result of experiments conducted on the rarefied facility Marhy from Icare laboratory and numerical simulations developed at the IUSTI laboratory. This work focuses on the study of plasma actuator effects having an influence on the aerodynamic properties of a rarefied Mach 2 air flow interacting with two different model geometries: a cylinder and a flat plate. For both cases the plasma actuator consists on a plasma discharge created by means a Spellman high voltage power supply delivering a DC voltage up to 20 kV and 400 mA, applied on the surface of the model. The aerodynamic changes produced by the plasma discharge is analysed with an iCCD camera and Pitot tube measurements. Optical emission spectroscopy and thermal infrared measurements helped the understanding of the observed effects. The main result is that depending on the geometry of the model, the greater cause due to the plasma actuator is not the same, despite the fact that the nature of the plasma discharge and the flow properties are the same. In the case of the flat plate, it was observed a thickening of the boundary layer, and then an increase of the shock angle of around 4-7 %. Numerical simulations, validated with the experimental measurements showed that this effect is due to the heating of the surfaced plate produced by the plasma. In the case of the cylinder, it was experimentally observed an increase of the standoff distance of the shock, which depends on the electrical power discharge. Thermal effects due to a local surface heating cannot explain the observed modification of the shock shape. It is shown that this modification seems to strongly depend on the ionisation rate of the plasma region whereas the discharge is applied modifying the local isentropic coefficient.

1. Introduction

This paper deals with the topic of supersonic flow control by means of plasma actuators. The aim is to manipulate a flow to a desired change[1]. The electrohydrodynamic actuators seem to be good candidates compared to the traditional active flow control method. Flow control by plasma actuators is a field of research really in vogue these days even though as early as the beginning of the 80s anomalous behaviors of shock waves in front of bodies traveling in weakly ionized gases have been reported [2]. The possibilities of application of such a method in aerodynamic field are very wide. The main advantages of plasma airflow control compared to mechanical actuators are the lack of moving parts and the short response time [3, 4]. A review of airflow control by non-thermal plasma actuators is given in [3]. In supersonic flow condition, the physical mechanisms responsible for aerodynamics effects resulting from electrical discharges created in air flow is commonly interpreted in terms of heat release associated with Joule heating [5, 6, 7]. Reviews of plasma applications in high speed aerodynamics were presented in [6, 7]. Nevertheless they remain experiments which can hardly be explained [3] and [8, 9, 10, 11, 12]. This argument is especially true for the experiments in which a change in the polarity of the discharge results in a change of the effect [8, 12]. The quantification of the non thermal mechanisms is important for future applications and at the same time it is very hard because they act in addition to the gas heating effect and the Joule heating can overshadow other effects [13, 14, 15]. This paper presents a joined effort between numerical simulation and experiments in order to have better understanding of all the phenomena involved. This study follows previous works presented in [4, 16, 17, 18], and allows a better understanding of the nature of the interaction between the flow and the discharge for two different geometrical set up.

Stagnation conditions	Flow conditions
$P_0 = 63Pa$ $T_0 = 30K$ $\rho_0 = 7.44 \cdot 10^{-4} kg.m^{-3}$	$P_\infty = 8Pa$ $T_\infty = 163K$ $\rho_\infty = 1.71 \cdot 10^{-4} kg.m^{-3}$ $M_\infty = 2$ $\lambda_\infty = 0.375mm$ $q_m = 3.34 \cdot 10^{-3} kg.s^{-1}$

Table 1: Flow conditions for an 8 Pa Mach 2 nozzle.

It is demonstrated that the nature of the interaction is much different for the two case and so strongly related to the nature of the shock wave. First we will present the experimental facility where the measurements have been carried out. In a second part we shall describe the fluid mechanic equations used to describe the flow and the numerical method used to perform the calculation. The third part is concerns the validation of the numerical approach, for the two test cases. Then the interaction between the discharge and the flow is studied, once again for the two geometries. Finally we conclude and give some perspectives.

2. Experimental set up

The experimental arrangement involves the supersonic wind tunnel MARHy (Mach adaptable rarefied hypersonic, figure 1), the model, the Pitot tube robe and the high voltage power supply.

Each experiment is performed in the wind tunnel MARHy which delivers supersonic and hypersonic flows at low pressure. The wind tunnel MARHy offers a wide range of Mach numbers (from 0.8 to 20) and Reynolds numbers (from 250 to 8000 for 10 cm reference length), in a circular test section of a 100 mm in diameter. Moreover, it has the particularity to run continuously thanks to a powerful pumping group allowing a mass flow rate of up to 4 gs^{-1} , which works properly (in an adapted mode) with a reservoir pressure of 63 Pa and a chamber pressure of 8 Pa is used. In the free stream, the flow conditions given in Table 1 are then achieved. These conditions simulate a high altitude flight, about 80 km, at high velocity 511 m/s.

The model under investigation is a quartz flat plate with a sharp leading edge. It is 90 mm long, 80 mm wide and

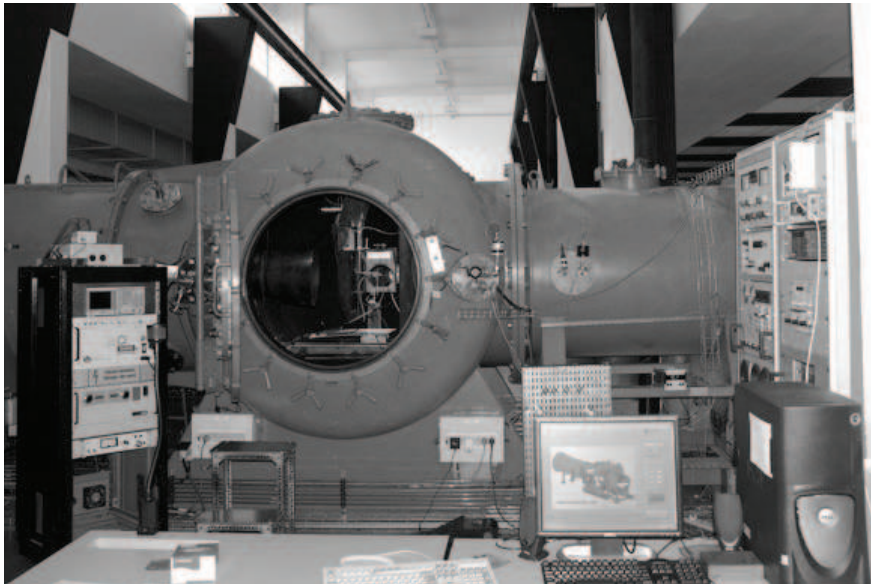


Figure 1: Wind tunnel MARHy.

4 mm thick. Figure 2 shows a schematic representation of the flat plate with its dimensions. Two 35 mm wide flush mounted aluminum electrodes are glued on the upper surface of flat plate. The first electrode is placed at 5 mm from the leading edge and the second electrode is placed at 5 mm from the trailing edge. It is 0.5 mm thick and the space between the two electrodes is 20 mm.

The discharge is created between the upstream electrode, carried to a negative voltage, and the downstream electrode

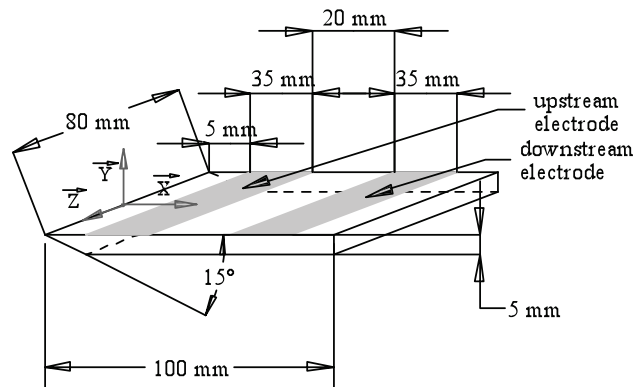


Figure 2: Schematic representation of the flat plates used with electrode.

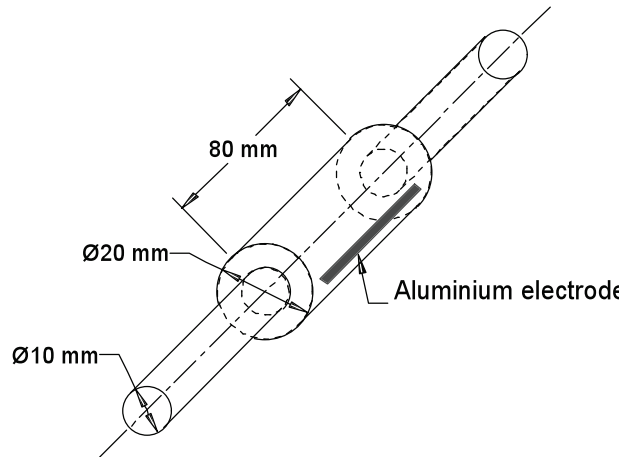


Figure 3: Schematic representation of the cylinder used with electrode.

connected to the ground, as the wind tunnel is. In the following part the upstream electrode is named the active electrode. Despite the big diameter of the wind tunnel (4 m), from an electrical point of view, the wind tunnel could interact with the active electrode because they are plugged to the same potential. A detailed description can be found in [20]. The negative high voltage is obtained with a Spellman high voltage power supply, delivering up to 15 kV and 400 mA. The power supply is used in voltage regulated mode. The accuracy given by the power supply is 10 V for the mean voltage and 1 mA for the current. In our experiment we have fixed three operating power discharges: 30 W ($U=-1.07$ kV, $I=28$ mA), 60 W ($U=-1.34$ kV, $I=45$ mA) 90 W ($U=1.68$ kV, $I=58$ mA). The Pitot probe is made of glass in order to avoid electrical interactions with the discharge. It has an outer diameter of 6 mm and an inner diameter of 4 mm, which is sufficient to avoid rarefaction effects [16, 17]. The tube is connected to a Mks BARATRON type 626 AX 01 TBE absolute pressure transducer. It covers a range from 0 to 133 Pa with an accuracy of 0.25% of the reading. The position of the Pitot probe is controlled with a three dimensional translator itself controlled by a computer. Figure 4 shows the experimental configuration. As the numerical simulation takes into account the temperature of the plate, the infrared thermography diagnostic is used in order to measure the temperature of the upper face of the plate. The distribution of the temperature over the surface of the flat plate is obtained with an infrared camera ThermoCAM MSC 3000 by FLIR laid on the top of the wind tunnel. The measurements are obtained through a fluorine window compatible with Ir wavelength range. The camera is equipped with an infrared photo detector is of QWIP type (quantum well infrared detector) constituted of 320×240 pixels, and working in the wavelength region ranged between the $8 \mu\text{m}$ and $9 \mu\text{m}$ corresponding to the temperatures ranged between -20 and 1500 °C. Intrinsic precision of the camera is 0.1 °C. But uncertainty is mostly due to the emissivity value of the materials and which is an input parameter of the camera software. An emissivity value equal to 1 has been taken for the quartz. But the electrodes of aluminum act as a body

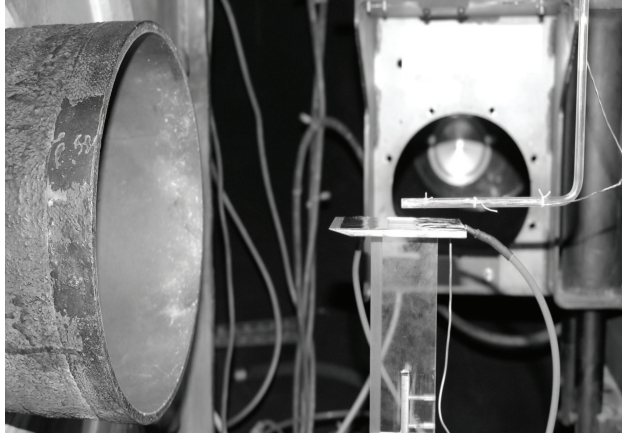


Figure 4: Experimental configuration.

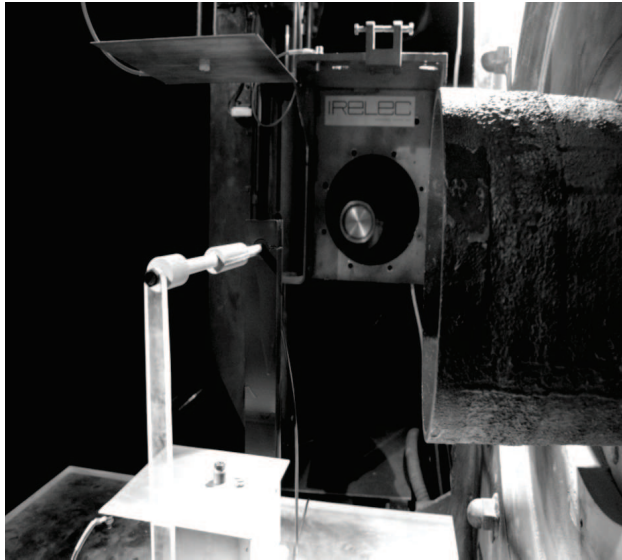


Figure 5: Experimental configuration.

with no intrinsic emissivity; they just reflect the temperature of the elements around like a mirror. For the electrode temperature measurements it is necessary that they return its own temperature. So it was decided to paint a small area of the electrodes with high resistive temperature black paint. As the painting emissivity value is not well known (ranges between 1 or 0.95) it leads to a difference of 5°C in the temperature results. This value can thus be considered as the accuracy of the temperature measurements. A complete description of the measuring technique can be found in [21]. During the whole experiment, the surface temperature is acquired to ensure that those measurements are done when the thermal equilibrium is reached (surface temperature and pressure measurements).

3. Fluid Mechanic Model

3.1 Governing Equations

In order to describe the air flow we use the 2D full compressible Navier-Stokes equations in the conservation form:

- the continuity equation :

$$\frac{\partial \rho}{\partial t} + \frac{\partial \rho u_i}{\partial x_i} = 0, \quad (1)$$

where x_i is the space coordinates, t is the time, ρ is the density and u_i is the velocity in the space direction x_i .

Parameter	He	N ₂	Air
σ_T [?]	1.004	0.923	-

Table 2: The measured values of coefficient σ_T .

- the momentum conservation equation :

$$\frac{\partial \rho u_j}{\partial t} + \frac{\partial (\rho u_j u_i + p \delta_{ij} - \tau_{ij})}{\partial x_i} = 0, \quad (2)$$

where p is the pressure, τ_{ij} the viscous shear stresses tensor and δ_{ij} Kronecker's symbol. We suppose that the fluid is Newtonian, so the viscous shear stresses tensor can be written as:

$$\tau_{ij} = \mu \left(\frac{\partial u_i}{\partial x_j} + \frac{\partial u_j}{\partial x_i} \right) - \delta_{ij} \frac{2}{3} \mu \frac{\partial u_k}{\partial x_k}, \quad (3)$$

here μ is the viscosity coefficient [22, 23].

- the energy conservation equation:

$$\frac{\partial \rho e_t}{\partial t} + \frac{\partial (\rho u_i e_t + u_i p - u_i \tau_{ij} + q_i)}{\partial x_i} = 0, \quad (4)$$

where e_t is the total energy $e_t = e + 1/2 \rho \sum u_i^2$, e is the internal energy, and q_i is the heat flux in the space direction i . As we work with air the Prandtl number is equal to 0.7.

This system closure is ensured by the equation of perfect gases :

$$p = \rho \frac{R}{\mathcal{M}} T, \quad (5)$$

where \mathcal{M} is the molar mass and R is the constant of perfect gases.

3.2 Rarefaction modeling

The boundary conditions for the equation system (1) – (4) are the slip velocity and the temperature jump conditions on the solid wall. This choice has been made to take into account the rarefaction effects which are non negligible in this case. Considering Knudsen number first order conditions only, the complete slip boundary condition reads [24]

$$u_s = -\sigma_p \frac{\mu}{p} v_m \left(\frac{\partial u}{\partial y} \right)_w + \sigma_T \frac{\mu}{\rho} \left(\frac{\partial \ln T}{\partial x} \right)_w, \quad (6)$$

where $v_m = \sqrt{2\mathcal{R}T_w(x)}$ is the most probable molecular velocity at the surface temperature T_w ; σ_p is the slip velocity coefficient and σ_T is the thermal slip coefficient. In this paper we use the velocity slip coefficient $\sigma_p^K = 1.012$ given in [24], under the full accommodation assumption. This value, taking into account the Knudsen layer influence, is also close to the one proposed in [?] $\sigma_p^C = 1.016$. Concerning the thermal slip coefficient σ_T numerous theoretical data are summarized in [25]. Measurements of this thermal slip coefficient for various gases are carried out in [?], it is important to note that measurements have only been made for pure gases : there are no experimental data for gas mixture. These measured values are given in Table 2. In the present work the well known value of σ_T , suggested in [24] and equal to 0.84, the calculated helium value from [25] ($\sigma_T = 1.175$), and also the measured air value from [?], are used. In this study the second term in equation (6) has not been taken into account because the first term of the equation is the predominant one and also as it was previously discussed, because all the σ_T measurements were made for pure gas. It is possible to try to extend the measurements to gas mixtures but it would lead to some uncertainties. Last but not least we have chosen to describe the plate as isothermal so there is no need to care about the σ_T value in our case and it was shown that. As this hypothesis gives good results (cf results paragraph).

Finally a boundary condition proposed by [24] has been chosen to describe the temperature jump at the wall:

$$T_s - T_w = -\xi_T \frac{\mu}{p} v_m \left(\frac{\partial T}{\partial y} \right)_w, \quad (7)$$

Parameter	<i>He</i>	<i>N₂</i>	<i>Air</i>
viscosity(μ_{ref}) ($10^{-5} Pa \cdot s$)	1.865	1.656	1.709
viscosity index (ω)	0.66	0.74	0.76
specific gas constant (\mathcal{R}) ($J \cdot kg^{-1} \cdot K^{-1}$)	2077.	297.	287.
$A(\omega)$	1.112	1.034	1.014
ratio of specific heats (γ)	1.67	1.4	1.4

Table 3: Physical constants of the gases under standard conditions.

where ξ_T is the temperature jump coefficient. For this coefficient, [26] and then [27] proposed a first expression of ξ_T . In this work we have used the expression proposed by [24] under diffuse reflection assumption and taking into account the Knudsen layer effect $\xi_T = 1.173 \frac{\gamma}{4(\gamma-1)} \frac{\sqrt{\pi}}{Pr}$. Similar values of the temperature jump coefficient were obtained by [28].

Furthermore the mean free path is usually written as a function of macroscopic parameters

$$\lambda = k_\lambda \frac{\mu}{p} \sqrt{\mathcal{R}T},$$

where the coefficient k_λ depends on the molecular interaction model. A very usual choice [?] consists in retaining $k_\lambda = \sqrt{\pi}/2$, i.e. a value close to that obtained from the hard sphere model (HS) [29]. In the present study we retain $k_\lambda = A(\omega) = \frac{2(7-2\omega)(5-2\omega)}{15\sqrt{2\pi}}$, the expression used in [30] for the variable hard sphere model (VHS), more general than the HS model, where the coefficient $A(\omega)$ depends only on the type of gas (see Table 3).

4. Numerical Procedure

4.1 Numerical scheme

The finite volume approach is used to solve the system numerically(1)-(4). This system is written in a vector form :

$$\frac{\partial \mathbf{U}_v}{\partial t} + \text{div} [\mathcal{F}(\mathbf{U}_v)] = 0, \quad (8)$$

where \mathbf{U}_v is the conservative variable vector:

$$\mathbf{U}_v = (\rho, \rho u_1, \rho u_2, \rho e_t)^T. \quad (9)$$

The numerical code utilizes structured multiblock grid based on the discretization of the unsteady compressible Navier-Stokes equations by an explicit cell centered finite volume method. The flux vector $\mathcal{F}(\mathbf{U}_v)$ may be decomposed into a convective and a diffusive parts. The convective (Euler) one is discretized using a second order accurate TVD-upwind, cell centered finite volume scheme based on an exact Riemann solver. The diffusive part is discretized with a second order finite difference scheme. A second order accurate scheme in time is obtained by using a predictor corrector approach.

4.2 Mesh

For the flat plate test case the computational domain is divided into 7 blocks and the total number of cells is 166,000. For the cylinder one, The computational domain is divided into 8 blocks of Q4, with a total number of 148,800 cells. The minimum space step of $\Delta x_{min} = 5.10^{-4}$ m, has been chosen as the result of the convergence study and also taking into account that the value of the mean free path in the free stream is $\lambda = 2.7.10^{-4}$ m.

4.3 Boundary Conditions

The classical boundary conditions is : no reflection or zero gradient ones for the north, east and south, supersonic inflow for the west. For the velocity slip and temperature jump conditions at the wall of the plate, a semi-implicit treatment is used.

4.4 Discharge modeling

For the flat plate case the discharge action on the flow is modeled via a surface temperature increase. The temperature distribution has been measured by the IR camera (cf : figure 6). For the cylinder case the surface heating and the

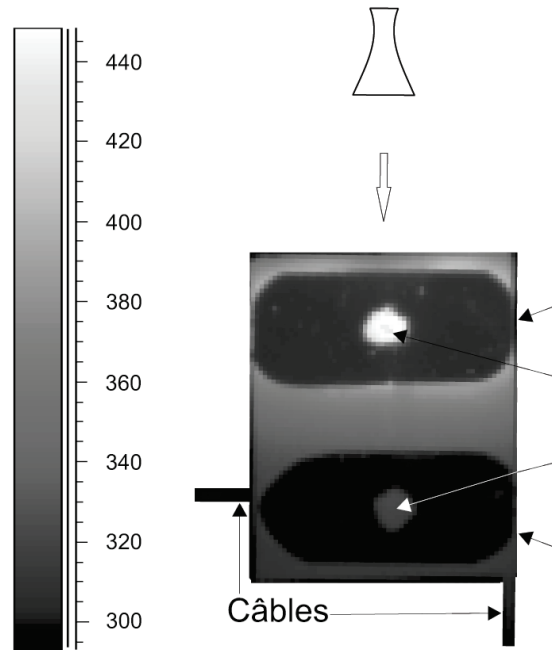


Figure 6: IR camera measurement example.

volumetric has been investigated with the numerical code as shown on figure 7. Some non equilibrium modeling based on Ambrosio and Wortman [31] approach adapted to plasma discharge case by Burm et al [32, 33] was considered to explain the discharge effects.

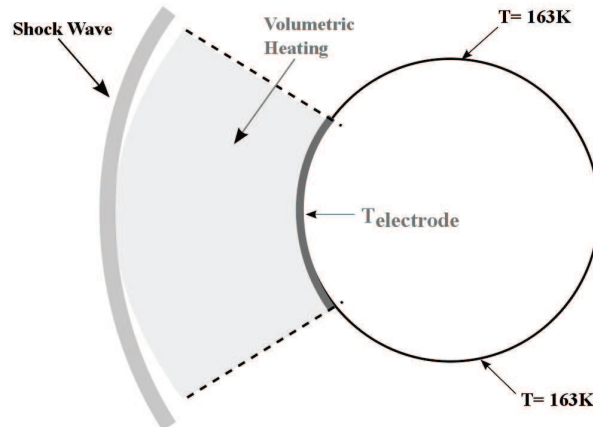


Figure 7: Surface and volume heating descriptions

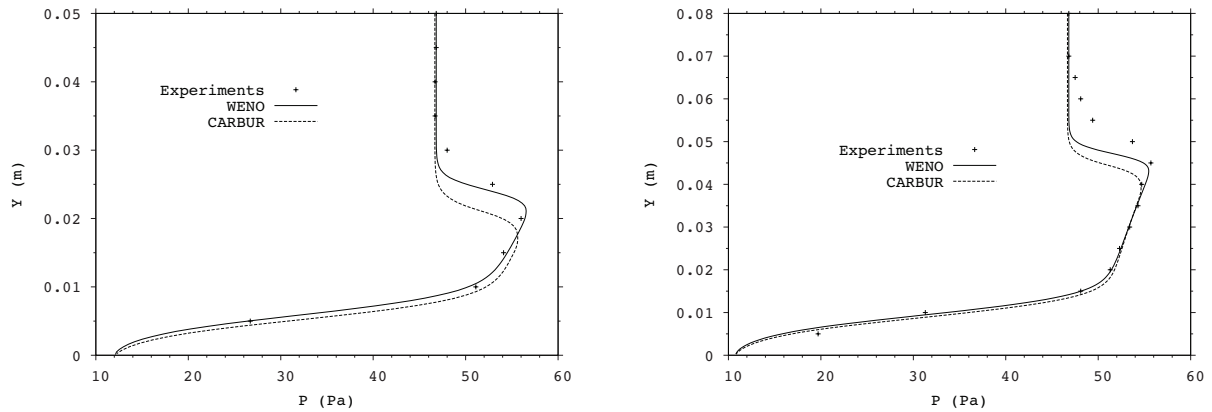


Figure 8: Total (Pitot) pressure profile for $x=22\text{mm}$ and 50mm without discharge.

5. Results

5.1 Validations

For the two geometrical configurations calculations without any discharge have been carried out and compared to experimental data in order to validate the numerical code, especially for the rarefaction modeling effects. Figures 8

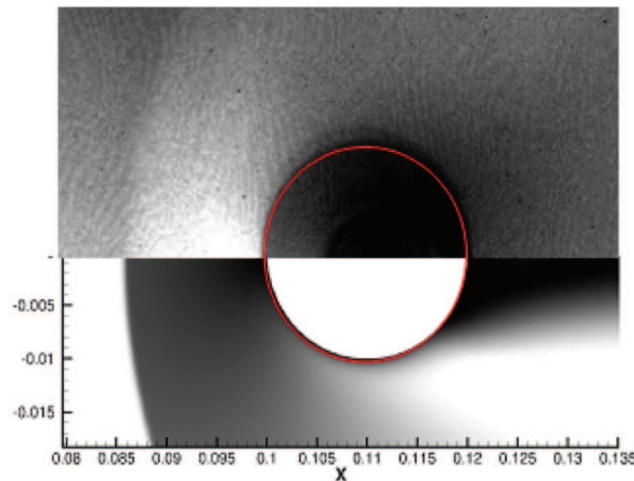


Figure 9: Shock wave position, comparison between experiment and simulation, without discharge.

and ?? clearly demonstrate the capabilities of the numerical code to simulate that kind of flow even if the rarefaction effect is quite important.

5.2 Flat plate test case

In this case the interaction between the electric discharge and the flow is modeled by pure thermal surface heating, and unlike in previous work the temperature gradient along the plate is now taken into account (cf : figure 10). Figure 11 shows the experimental Pitot pressure profiles compared to those obtained numerically with the temperature distribution models and a constant temperature for the plate [18], for a 90W upstream discharge. These results show that even if the interaction between the flow and the discharge is mainly due to a surface heating there are also other phenomena involved like volumetric heating and dissociation, ionization and thermal non equilibrium between electrons and heavy species. The isothermal hypothesis allows emulating the overall interaction.

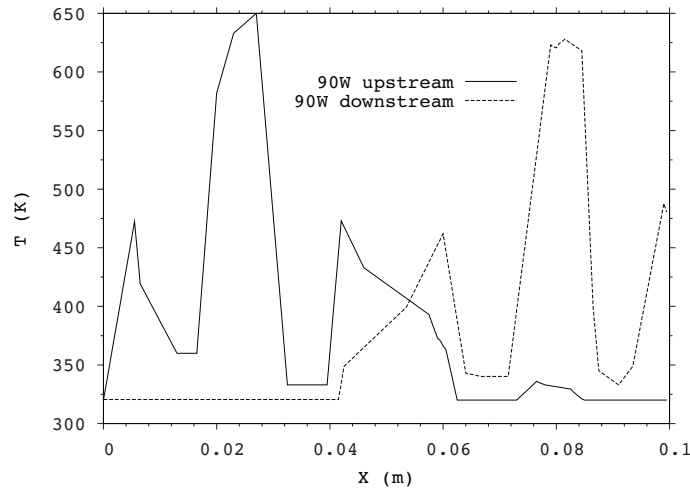


Figure 10: Temperature distribution over the flat plate for the 90W upstream and downstream cases.

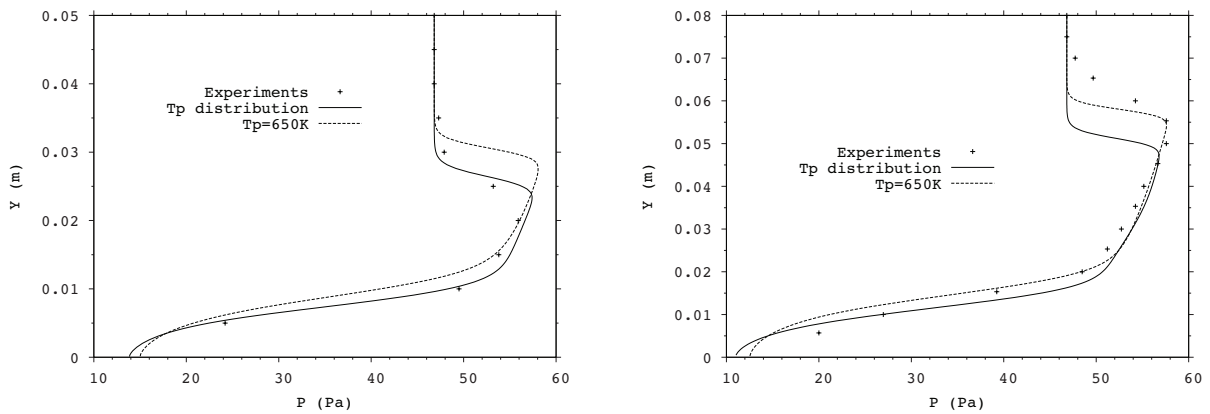


Figure 11: Total (Pitot) pressure profile for $x = 22\text{mm}$ and 50mm with a 90W upstream discharge.

Figures 12 shows the experimental Pitot pressure profiles compared to those obtained numerically with the temperature distribution models and a constant temperature for the the plate [18], in case of a 90W downstream discharge. These results exhibits that the isothermal hypothesis is not valid for the downstream case and even if the numerical results obtained with the non-uniform temperature distribution allows to describe correctly the overall interaction between the discharge and the flow. One main conclusion of this study is: the maximum temperature has an impact on the flow but its location is much more important.

5.3 Cylinder test case

First the surface heating was investigated, in order to reproduce a 5.8% stand-off modification but calculations show that the surface temperature must be increased up to 1000K. So it is obvious that surface heating is not able to reproduce the experimental observations.

The volumetric heating was also studied. From figure 13 one can see that the stand-off evolution as a function of the electric discharge power is linear as well as in the experimental case than in the numerical one. Nevertheless there is more than one order of magnitude between the two cases, so it could mean that the energy efficiency is very poor.

Figure 14 shows that there is a quite strong electronic non equilibrium, meaning that the equilibrium hypothesis is not

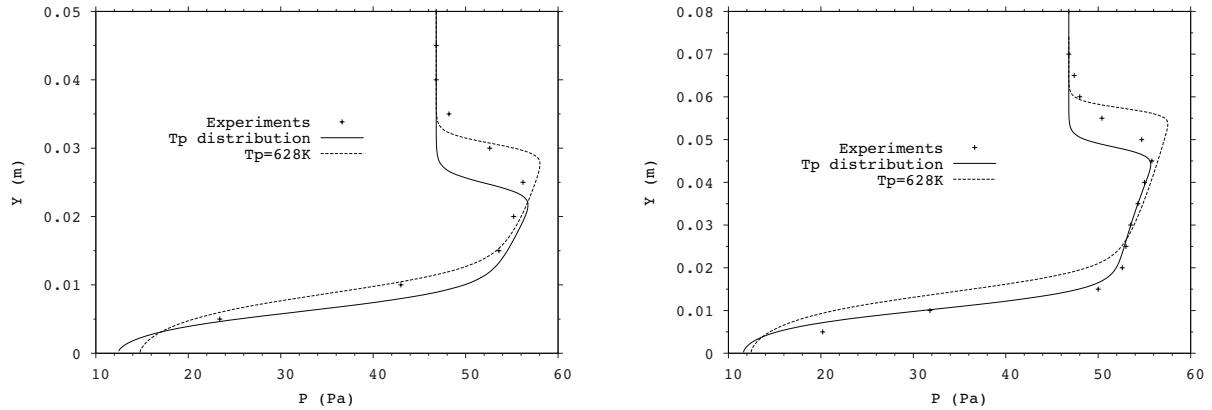


Figure 12: Total (Pitot) pressure profile for $x=22\text{mm}$ and 50mm with a 90W downstream discharge.

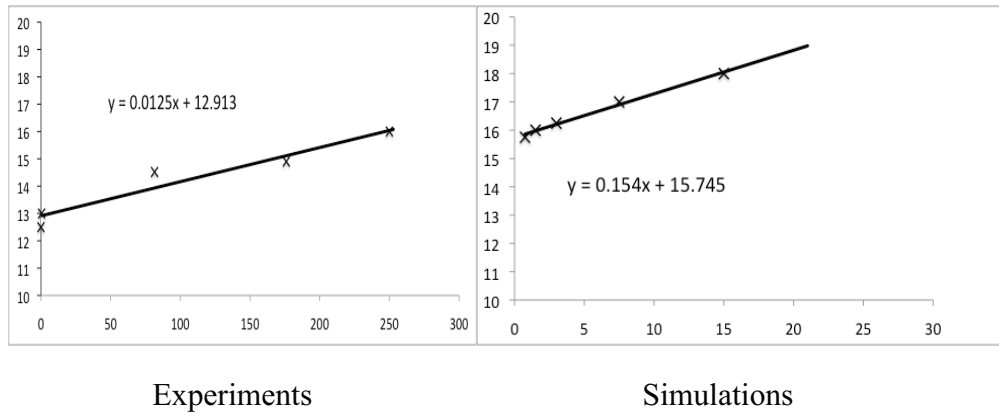


Figure 13: Stand-off evolution vs Discharge Power.

valid. Moreover one can see that measured temperatures are almost constant which is not the case for the numerical simulations. As a conclusion we can say that the volumetric heating is not involved in the interaction between the flow and the discharge and that the electronic non-equilibrium must be taken into account. To validate this assumption the Ambrosio and Wortman [31] approach adapted to plasma discharge case by Burm et al [32, 33] has been used and completed by experimental observations. Results from these calculations are presented on figure 15. The values obtained are between 15.3mm and 17.3mm , which are close to those determined experimentally validating this approach.

6. Conclusions and Perspectives

This study has shown that the nature of the interaction between a supersonic rarefied flow and electric discharge strongly depends on the studied geometry and as a consequence on the nature of the shock wave involved. It was also demonstrated that for a given geometry the nature of the interaction depends of the location of the discharge. One of the major facts of the study is that electronic non-equilibrium should be modeled in most of the cases and that the Ambrosio's approach is able to describe the interaction. Consequently, the first perspective will be to try to extend it to the flat plate case and then add this model in the numerical code developed by the authors.

References

- [1] M. Gad-El-Hak *Flow control*, Cambridge University Press, UK, 2000.

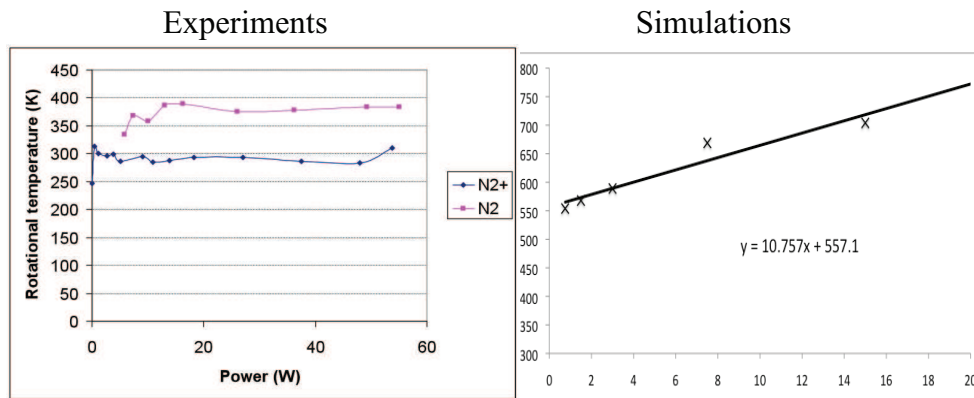


Figure 14: Temperatures vs Discharge Power.

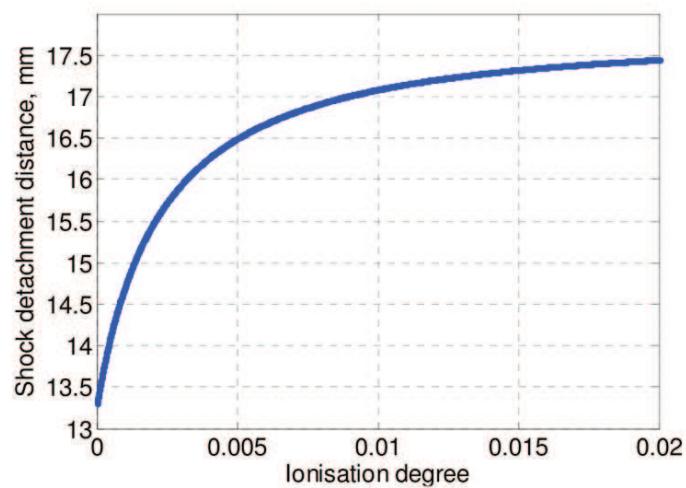


Figure 15: Shock wave detachment distance calculated as a function of the ionization degree.

-
- [2] Fomin, V. M., Tretyakov, P. K., and Taran J. -P. *Flow control using various plasma and aerodynamic approaches (Short review)*, Aerospace Science and Technology, 8, 2004.
- [3] E. Moreau *Airflow control by non-thermal plasma actuators*, J. Phys D: Appl Phys., Vol. 40, pp. R605-R636, 2007.
- [4] E. Menier, L. Leger, E. Depussay, V. Lago and G. Artana *Effect of a dc discharge on the supersonic rarefied air flow over a flat plate*, J. Phys D, Vol. 40, pp. 695-701, 2007.
- [5] Menart J., Shang J. Atzbach C. Magoteaux, Slagel M., Bilheime *Total drag and lift measurement in a mach 5 flow affected by a plasma discharge and a magnetic field*, AIAA paper 2005-947, 2005.
- [6] P. Bletzinger, B.N. Ganguly, D. Van Wie and A. Garscadden *Plasmas in high speed aerodynamics*, J. Phys. D: Appl. Phys., Vol. 38, pp. R33-R57, 2005.
- [7] V.E. Semenov, V.G. Bondarenko, V.B. Gildenburg, V.M. Gubchenko and A.I. Smirnov *Weakly ionized plasma in aerospace application*, Plasma Phys. Control Fusion, Vol. 44, pp. 239-305, 2002.
- [8] A. Klimov, V. Bityurin and Yu Serov *Non-thermal approach in plasma aerodynamics*, AIAA paper n^o2001-0348, 2001.
- [9] V.A. Bityurin and A.I. Klimov *Non-thermal plasma aerodynamics effects*, AIAA paper n^o2005-0978, 2005.
- [10] S.B. Leonov, D.A. Yarantsev., V.G. Grommov and A.P. Kuriachy *Mechanisms of flow control by near surface electrical discharge generation*, AIAA paper n^o2005-780, 2005.
- [11] J. Shin, V. Narayanaswamy, L. Raja, N. T. Clemens *Characteristics of a plasma actuator in Mach 3 flow*, AIAA paper n^o2007-788.
- [12] J. Shin, V. Narayanaswamy, L. Raja, N. T. Clemens *Characterization of a Direct-Current Glow Discharge Plasma Actuator in low-Pressure Supersonic Flow*, AIAA Journal, Vol. 45, No. 7, pp. 1596-1605, 2007.
- [13] S. O. Macheret, M. N. Shneider and R. B. Miles *Magneto- hydrodynamic and electrohydrodynamic control of hypersonic flows of weakly ionized plasma*, AIAA Journal, Vol. 42, No. 7, pp. 1378-1387, 2004.
- [14] J. Shang, R. Kimmel, J. Menart, S. Surzhikov *Hypersonic Flow Control Using Surface Plasma Actuator* Journal of Propulsion and Power 2008 0748-4658 vol.24 no.5 (923-934).
- [15] J. Shang *Surface Direct Current Discharge for Hypersonic Flow Control*, Journal of Spacecraft and Rockets 2008 0022-4650 vol.45 no.6 (1213-1222) doi: 10.2514/1.37009.
- [16] E. Menier *Influence d'une Décharge électrique Continue sur un écoulement Supersonique Rarefié*, Ph.D. thesis, University of Orléans, France, 2007.
- [17] E. Menier, J.C. Lengrand and V. Lago *DSMC estimate of the ionic wind effect on a supersonic low-density flow*, 25th Intern. Sympos. Rarefied Gas Dynamics, Russia, 2006.
- [18] J. D. Parisse, L. Léger, E. Depussay, V. Lago, and Y. Burtschell *Comparison between Mach 2 rarefied airflow modification by an electrical discharge and numerical simulation of airflow modification by surface heating*, Physics of Fluids 22, 061703 2010.
- [19] Lago V., Depussay E., Lasgorceix P., Lebehot A., Martin J.P. *The experimental facilities at Laboratoire d'Aérodynamique*, 24th International Symposium on Rarefied Gas Dynamics, edited by M. Capitelli, American Institute of Physics, 2005, pp.1337-1340.
- [20] L. Léger, E. Depussay and V. Lago *D.C. Surface Discharge Characteristics in Mach 2 Rarefied Airflow*, Transaction on Dielectric and Electrical Insulation, 2009.
- [21] S. Mazouffre, P. Echegut and M. Dudeck *A calibrated infrared imaging study on the steady state thermal behaviour of Hall effect thruster*, Plasma Sources Sci. Technol. Vol. 16, pp. 13-22, 2007.
- [22] JANAF Thermochemical Tables, 3rd edition, M.W. Chase Jr., Davies C.A., Davies J.R., Fulrip Jr. D.J., McDonald R.A., and Syverud A.N., Journal of Physical and Chemical Reference Data, 14, Supplement 1, 1985.
- [23] Hirschfelder J.O., Curtiss C.F., Bird R.B. *Molecular Theory of Gases and Liquids*. John Wiley and Sons, 1954.

- [24] Kogan M.N. *Rarefied gas dynamics*, Plenum Press, New York, 1969.
- [25] S , F. Data on the velocity slip and temperature jump coefficients In *Thermal and Mechanical Simulation and Experiments in Micro-Electronics and Micro-Systems*, 5th Int.Conf. EuroSimE 2004 (ed. L.J. Ernst, G.Q. Zhang, P. Rodgers, O. de Saint Leger) pp. 243-249. Shaker Publishing.
- [26] V S M. *Über Wärmeleitung in verdünnten Gasen*, *Annalen der Physik und Chemie*, pp. 101-130, 1898.
- [27] K E. *Kinetic Theory of Gases*, McGraw-Hill Book Co., Inc., New York, 1938.
- [28] S F., *Application of the Cercignani-Lampis scattering kernel to calculations of rarefied gas flows. II. Slip and jump coefficients*, *Eur. J. Mech. B / Fluids*, 2003, v. 22, p. 133-143.
- [29] C , S. & C , T.G. 1970) *The mathematical theory of non-uniform gases* third edition, University Press, Cambridge.
- [30] B , G.A. *Molecular gas dynamics and the direct simulation of gas flows* Oxford University Press, New York, 1994.
- [31] A. Ambrosio, A. Wortman, *ARS Journal*, 32, 281 (1962).
- [32] K T A. Burm, W J Goedheer, D C Schram. *Physics of Plasmas*, 6, 2622-2627 (1999).
- [33] K T A. Burm, W J Goedheer, D C Schram. *Mach number for gases and plasmas in a convergent-divergent cascade arc*. *Physics of Plasmas*, 6, 2628- 2635 (1999).
- [34] G. N. Markelov, A. N. Kudryavtsev and M. S. Ivanov. *Continuum and kinetic simulation of laminar separated flow at hypersonic speeds*. *J. Spacecraft and Rockets*, 37 (4), pp.499-506 2000.
- [35] R. Donat and A. Marquina *Capturing Shock Reflections: An Improved Flux Formula*. *Journal of Computational Physics* 125, 42758 (1996).
- [36] Shang, J., Kimmel, R., and Hayes, J. *Study of surface and volume heating effects in a Mach 5 flow* , AIAA paper 2004-2262, 35th plasmadynamics and laser conference.
- [37] Menart J., Shang J. Atzbach C. Magoteaux, Slagel M., Bilheimer *Study of surface and volume heating effects in a Mach 5 flow*, *AIAA paper 2004-2262*, AIAA paper 2005-947, Reno, 2005.